



Article

Estimation of Evaporation and Drought Stress of Pistachio Plant Using UAV Multispectral Images and a Surface Energy Balance Approach

Hadi Zare Khormizi ¹, Hamid Reza Ghafarian Malamiri ² and Carla Sofia Santos Ferreira ^{3,4,*}¹ Faculty of Natural Resources, University of Tehran, Karaj 31587-77871, Iran; hadi.zarekh@ut.ac.ir² Department of Geography, Yazd University, Yazd 89158-18411, Iran; hrghafarian@yazd.ac.ir³ Polytechnic Institute of Coimbra, Applied Research Institute, Rua da Misericórdia, Lagar dos Cortiços—S. Martinho do Bispo, 3045-093 Coimbra, Portugal⁴ Research Centre for Natural Resources, Environment and Society (CERNAS), Polytechnic Institute of Coimbra, Bencanta, 3045-601 Coimbra, Portugal

* Correspondence: carla.ferreira@ipc.pt

Abstract: Water scarcity is a critical abiotic stress factor for plants in arid and semi-arid regions, impacting crop development and production yield and quality. Monitoring water stress at finer scales (e.g., farm and plant), requires multispectral imagery with thermal capabilities at centimeter resolution. This study investigates drought stress in pistachio trees in a farm located in Yazd province, Iran, by using Unmanned Aerial Vehicle (UAV) images to quantify evapotranspiration and assess drought stress in individual trees. Images were captured on 10 July 2022, using a Matrix 300 UAV with a MicaSense Altum multispectral sensor. By employing the Surface Energy Balance Algorithm for Land (SEBAL), actual field evapotranspiration was accurately calculated (10 cm spatial resolution). Maps of the optimum crop coefficient (K_c) were developed from the Normalized Difference Vegetation Index (NDVI) based on standard evapotranspiration using the Food and Agriculture Organization (FAO) 56 methodology. The comparison between actual and standard evapotranspiration allowed us to identify drought-stressed trees. Results showed an average and maximum daily evaporation of 4.3 and 8.0 mm/day, respectively, in pistachio trees. The real crop coefficient (K_c) for pistachio was 0.66, contrasting with the FAO 56 standard of 1.17 due to the stress factor (K_s). A significant correlation was found between K_c and NDVI ($R^2 = 0.67$, $p < 0.01$). The regression model produced a crop coefficient map, valuable to support precise irrigation management and drought prevention, considering the heterogeneity at the farm scale.

Keywords: UAV; SEBAL algorithm; crop water stress; irrigation management; arid region



Citation: Khormizi, H.Z.; Malamiri, H.R.G.; Ferreira, C.S.S. Estimation of Evaporation and Drought Stress of Pistachio Plant Using UAV Multispectral Images and a Surface Energy Balance Approach.

Horticulturae **2024**, *10*, 515. <https://doi.org/10.3390/horticulturae10050515>

Academic Editors: Kiril Bahcevandziev and José Manuel Monteiro Gonçalves

Received: 18 April 2024

Revised: 13 May 2024

Accepted: 15 May 2024

Published: 16 May 2024



Copyright: © 2024 by the authors. Licensee MDPI, Basel, Switzerland. This article is an open access article distributed under the terms and conditions of the Creative Commons Attribution (CC BY) license (<https://creativecommons.org/licenses/by/4.0/>).

1. Introduction

Water shortage is one of the main factors limiting the development of agriculture in arid and semi-arid regions. Water losses through evaporation and transpiration (ET) are an important part of the water cycle, and thus measuring and modeling these variables are very important [1,2]. Measuring ET is crucial in planning and managing water resources, optimizing crop production, and identifying crop drought/water scarcity stress [1,3]. ET can be measured using direct and indirect methods. Among the direct methods, one can refer to the use of lysimeters and water balance [4]. Traditional methods of measuring ET (e.g., lysimeter, eddy covariance, Bowen's ratio, FAO 56) are generally complex, costly, time-consuming, and point based [5,6]. Satellite data and remote sensing methods are increasingly employed for indirect ET measurements [7–10]. These data offer broad coverage, capturing heterogeneity and changes, while remaining cost-effective and featuring suitable time sequences and computer processing capabilities [11].

Numerous algorithms have been developed in recent decades for estimating ET using satellite image and remote sensing data. Surface Energy Balance System (SEBS) [12], Surface

Energy Balance Algorithm for Land (SEBAL) [13], Surface Energy Balance Index (SEBI) [14], Metric [15], and the Two-Source Energy Balance (TSEB) [16] are notable examples. The SEBAL algorithm, extensively utilized to calculate instantaneous surface energy balance in each satellite image pixel [17], is among the most widely adopted. The accuracy of the SEBAL algorithm in determining actual ET rates has been demonstrated in Iran [7,18–20] and studies worldwide [21–25].

While satellite images offer advantages in calculating ET, their use in assessing plant water stress, particularly in agriculture systems, has certain limitations. Notably, satellite images often exhibit low spatial resolution, especially in the thermal band range, limiting their suitability for precision agriculture and environmental applications [26]. Additionally, satellite transit times may not always align with research needs [4,27]. To address these limitations, Unmanned Aerial Vehicles (UAVs) or drones emerge as a promising platform for short-range remote sensing. Drones can operate in favorable weather conditions, providing flexibility in data collection, not always feasible with satellites. For example, the presence of clouds in satellite images is also an important challenge [28,29]. In this context, UAVs do not face this problem with flexibility in flight time and flying under cloud cover. Equipped with red, green, and blue wavelengths (RGB) cameras, multispectral cameras, and infrared thermal cameras, drones can capture images with significantly high spatial resolution, down to the centimeter scale. This enhanced resolution is crucial for detecting temporal and spatial changes in crops, allowing for precise observation of tree-level variations in water use and stress indicators, such as signs of water stress [26]. Furthermore, UAV images enable more accurate delineation of crown pixels from the soil background, overcoming some of the challenges associated with satellite imagery [30].

Presently, UAVs are widely and successfully employed in agricultural research, addressing areas such as water stress [31,32], weed separation [33,34], and pest control [35]. Numerous studies utilize drones for calculating ET. For example, Park et al. [26] measured the evapotranspiration of a peach orchard using multispectral and thermal images captured by a drone. The findings revealed a robust linear relationship (explanatory coefficient of 0.89) between estimated ET and leaf transpiration. The daily ET measured by UAV data differed by 5.50 mm from the crop's ET (6.35 mm), as determined by meteorological methods at the study site, representing a daily variation of 0.85 mm [26]. In a study focused on almond farms, ET was determined using UAV images and an integrated approach with Landsat 8 images employing the Metric algorithm. The results indicated a strong correlation between ET_{UAV} and Landsat 8-based METRIC [36]. Niu et al. [37] explored ET in pomegranate tree using multispectral drone images and lysimeter data. The crop coefficient (K_c) values were calculated based on actual ET from the lysimeter and the reference ET from the weather station. A linear regression model between K_c and the Normalized Difference Vegetation Index (NDVI) demonstrated the ability to estimate tree-level ET with a coefficient of determination (R^2) of 0.91 and mean absolute error (MAE) of 0.39 mm per day. Ortega-Farías et al. [38] investigated ET in olive orchard based on multispectral and thermal sensors on a UAV, along with the remote sensing energy balance (RSEB) algorithm. The results indicated a 13% overestimation of ET by RSEB compared to the eddy covariance (EC) method, with a root mean square error (RMSE) and average absolute error of 0.43 mm per day. Tang et al. [39] forecasted ET in corn using K_c derived from UAV multispectral images through the FAO 56 dual vegetation coefficient approach, yielding an RMSE of 0.95 mm per day. The current study aims to determine the actual ET rates of pistachio trees, and advances in the state of the art by identifying trees experiencing drought stress by using high spatial accuracy multispectral and thermal drone images. The outcomes of this research have practical implications for precision irrigation management by averting drought stress at the individual tree level within agricultural systems. This is of utmost importance to support crop yield in water-scarce areas and mitigate the impact of climate change.

2. Materials and Methods

2.1. Study Area

This study focuses on a pistachio farm situated in the southwest of Yazd province, Iran (Figure 1), at a latitude of $31^{\circ}15'15''$ and longitude $53^{\circ}23'43''$ from the prime meridian. The farm spans 477.5 ha and exclusively features the pistachio species (*Pistacia vera* L.). According to the meteorological station located in the farm, the average annual rainfall is 70 mm, the average annual temperature is 18.7°C and the minimum and maximum temperature are -12°C and 44°C , respectively, based on records from 2019 to 2023.

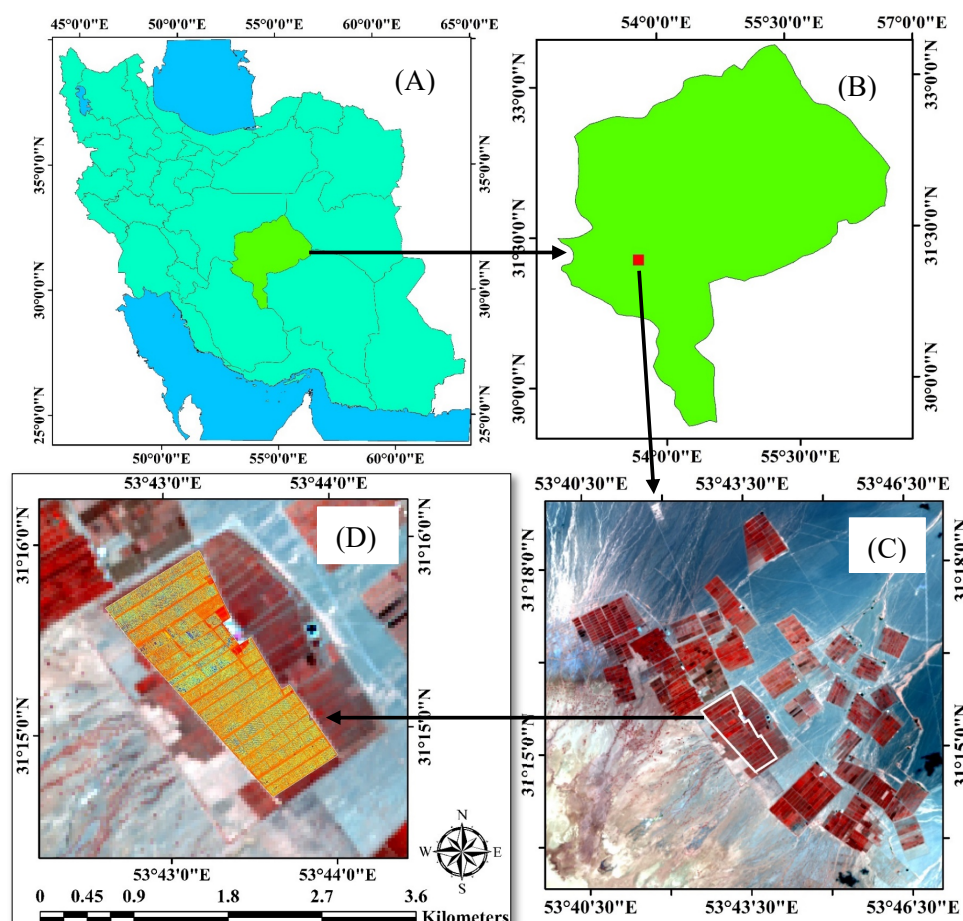


Figure 1. Location of the study area in Iran (A), Yazd province (B), pistachio orchards (C) and pistachio orchard investigated (D).

2.2. Data Collection with Drone

In the investigated farm, a plot of 207 ha (Figure 1D) was surveyed using a UAV on 10 July 2022. Images of the pistachio farm were captured using the DJI Matrice 300 RTK drone, equipped with the MicaSense Altum multispectral sensor (Figure 2). The MicaSense Altum sensor features five spectral bands spanning the blue, green, red, red edge, and near-infrared wavelengths, in addition to a thermal band (Table 1). Installed on the stabilizer system of the Matrix 300 UAV, the sensor facilitated automated image capture with predefined flight paths and areas stored in the UAV controller. The flight parameters included a longitudinal and transverse image overlap of 80% and 40%, respectively, at a flight altitude of 60 m. Although the longitudinal overlap does not affect the UAV's battery consumption, the increase in the transverse overlap enhances the flight lines and as a result increases the battery consumption. Longitudinal overlap was considered greater than transverse overlap. Additionally, to reach a pixel size of 40 cm for the thermal band, a height of 60 m was chosen for the flight. Flying at an altitude of 120 m resulted in a pixel

size of 80 cm for the thermal band, which was not accurate enough for small trees. Due to the extent of the surveyed plot and UAV battery limitations, the entire study area was photographed in six separate flights, each lasting approximately 25 min.



Figure 2. DJI Matrice 300 RTK drone (DJI, Frankfurt, Germany) and Altum MicaSense sensor used for image collection.

Table 1. Characteristics of the Altum MicaSense sensor.

Band Name	Band Center	Bandwidth	No Column × Row	Pixel Size at the Height of 60 m (cm)
Blue	475 nm	32 nm	2064 × 1544	2.6
Green	560 nm	27 nm	2064 × 1544	2.6
Red	668 nm	14 nm	2064 × 1544	2.6
Red Edge	717 nm	12 nm	2064 × 1544	2.6
Near Infrared	842 nm	57 nm	2064 × 1544	2.6
Thermal	11 μm	6 μm	160 × 120	40

Reflectance calibration panels were recorded before and after each flight to obtain coefficients for converting pixel values to reflection values based on weather conditions. The imaging took place from 10:30 a.m. to 13:30 p.m. This time range was chosen to minimize shadows in the images, taking advantage of the sun's angle, maximum air temperature, and stable air and soil surface temperatures. The selection aimed to ensure minimal half-hourly changes in the images, aligning with this study's objectives of estimating tree ET and assessing drought stress under consistent sun positioning and temperature stability.

Following the image collection, the images from each flight underwent conversion to reflectance values with the reflection calibration panel for pixel values of bands 1 to 5. It is important to note that the thermal band of the MicaSense Altum sensor is calibrated and does not require specific corrections. All bands of the images from the six flights in the study area were mosaiced. To standardize the pixel sizes of the thermal band with the spectral bands and alleviate the computational load, the pixel size for all measuring bands was adjusted to 10 cm.

2.3. Methodology

Generally, this study can be described in four steps. In the first step, the actual evapotranspiration (ET_a) is calculated using the SEBAL algorithm (Section 2.3.1). The

second step is to calculate the reference evapotranspiration of the plant and determine the relationship between NDVI and the instant crop coefficient ($K_{C_{int}}$) obtained through the SEBAL algorithm (Sections 2.3.2 and 2.3.3). The third step consists of obtaining the standard evapotranspiration through the relationship between the crop coefficient and NDVI (Section 2.3.3). And the fourth step is to obtain the drought stress map of the field by determining the difference between actual evapotranspiration with the standard (Figure 3). In general, these steps were developed in MATLAB R2023a software and maps were prepared using ArcGIS 10.8 software.

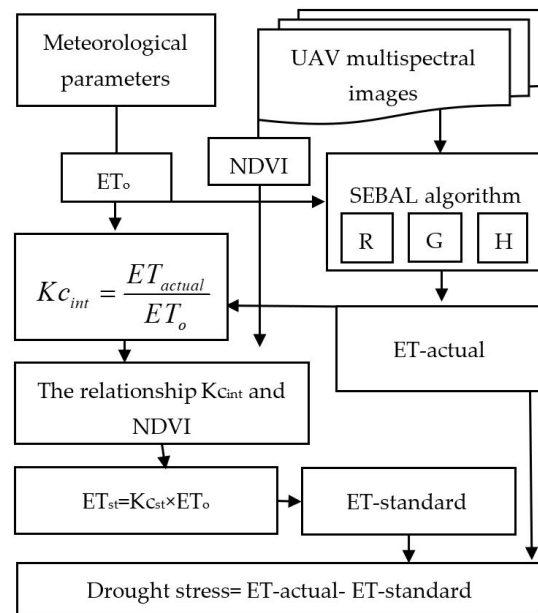


Figure 3. Methodological framework.

2.3.1. The SEBAL Algorithm for the Calculation of Real Evapotranspiration

The basis of the SEBAL algorithm is the use of energy balance equation and surface energy balance (Equation (1)). A comprehensive and complete explanation of each part of this algorithm, including its main parameters, are presented in Allen et al. [40]. In the SEBAL algorithm, the instantaneous value of latent heat of evaporation (λET_{inst}), is calculated as the remainder of the energy balance equation (Equation (1)) for each pixel [13].

$$\lambda ET_{inst} = R_n - G_0 - H \quad (1)$$

where λET_{inst} is the latent heat flux of evapotranspiration (W/m^2), R_n is the net solar radiation (W/m^2), G_0 is the soil heat flux (W/m^2), and H is the sensible heat flux (W/m^2).

Net Solar Radiation (R_n)

In the SEBAL algorithm, net solar radiation is calculated from the balance of four radiation fluxes, which include incoming short-wave radiation ($R_{S\downarrow}$), outgoing short-wavelength reflection ($R_{S\uparrow}$), incoming long-wavelength radiation ($R_{L\downarrow}$) and emission long-wavelength radiation from the surface ($R_{L\uparrow}$). Instantaneous net radiation per unit area is calculated using Equation (2).

$$R = (1 - \alpha)R_{S\downarrow} + R_{L\downarrow} - R_{L\uparrow} - (1 - \varepsilon_0)R_{L\downarrow} \quad (2)$$

where α is the surface albedo and ε_0 is the surface emissivity. ε_0 is obtained according to the surface vegetation conditions.

In the present study, the albedo of the surface was calculated using Equations (3) and (4) based on data collected with the Altum MicaSense sensor [35].

$$\alpha = 0.526 \times VIS + 0.474 \times NIR, \quad \text{for } NDVI < 0.25 \quad (3)$$

$$\alpha = 0.526 \times VIS + 0.362 \times NIR + 0.112(0.5 \times NIR), \quad \text{for } NDVI \geq 0.25 \quad (4)$$

where VIS is the reflectance of the visible bands and NIR is the reflectance of the near infrared band. Equation (3) is applied in areas with NDVI value lower than 0.25, whereas Equation (4) is used for areas with NDVI value higher than 0.25. NDVI was calculated according to Equation (5) [41].

$$NDVI = \frac{NIR - RED}{NIR + RED} \quad (5)$$

where NIR and RED are spectral reflectance of the near infrared and the red band, respectively. The obtained range of this index varies from -1 to $+1$. Negative values indicate clouds and water, positive values near zero indicate bare soil, values ranging from 0.1 to 0.5 indicate sparse vegetation and values ≥ 0.6 specify dense green vegetation [40].

Ground Heat Flux (G_0)

It is difficult to directly calculate ground heat flux using satellite images. In this regard, the relationship between G_0/R_n ratio and parameters such as NDVI and surface temperature (T_s) are used to calculate ground heat flux. In SEBAL method, the G_0/R_n ratio in half a day is calculated using the empirical relationship provided by Equation (6) [17,40].

$$\frac{G_0}{R_n} = \frac{T_s}{\alpha} (0.0038\alpha + 0.0074\alpha^2)(1 - 0.98NDVI^4) \quad (6)$$

where T_s is the surface temperature ($^{\circ}\text{C}$), α is the surface albedo and NDVI is the normalized difference index of vegetation cover.

Sensible Heat Flux (H)

To estimate the sensible heat flux in the SEBAL algorithm, two threshold pixels are selected. One of these pixels, which is called a cold pixel, is associated with an area completely covered with plants and irrigated, where land surface temperature is close to the air temperature, and ET is equivalent to the ET of the reference plant. The second pixel, which is called a warm pixel, is an agricultural land without vegetation and dry. Therefore, the latent heat flux of evaporation in this pixel is assumed to be zero. In SEBAL method, according to Equation (1) and based on the values of ET of the mentioned two pixels, the sensible heat flux is calculated in these two pixels and then the sensible heat flux of other pixels is estimated. The amount of sensible heat flux is estimated by Equation (7) [40].

$$H = \frac{\rho \times C_p \times dT}{R_{ah}} \quad (7)$$

where ρ is the air density (kg/m^3), C_p is the specific heat of air ($\text{J}/\text{kg}/\text{k} = 1004$), dT is the air temperature difference near the surface (k) and R_{ah} is the aerodynamic resistance for heat transfer (s/m).

Calculation of Instantaneous and Daily Evapotranspiration

After calculating the main parameters of the SEBAL algorithm, the instantaneous value of the latent heat flux of ET is calculated for each pixel according to Equation (1). Then, the instantaneous value of ET is obtained using Equation (8).

$$ET_{inst} = 3600 \frac{\lambda ET_{inst}}{\lambda} \quad (8)$$

where ET_{ins} is instantaneous evapotranspiration (mm/hr), λ is the latent heat of evapotranspiration (J/kg), and the number 3600 is the time conversion factor from seconds to hours.

After calculating ET_{ins} , the reference ET fraction is calculated using Equation (9). Then, the actual daily evaporation is obtained by multiplying the reference ET fraction by the daily ET value of the reference plant (Equation (10)).

$$ETrF = \frac{ET_{int}}{ET_{r-int}} \quad (9)$$

$$ET_{24h} = ETrF \times ET_{r-24} \quad (10)$$

where $ETrF$ is the fraction of reference evapotranspiration, ET_{r-int} is instantaneous reference plant evapotranspiration (mm/hr), ET_{r-24} is daily reference plant evapotranspiration (mm/day) and ET_{24h} is actual daily evapotranspiration (mm/day).

2.3.2. Estimation of Reference Evapotranspiration of the Plant

The ET of the reference plant can be calculated via different methods. In the present study, the Penman–Monteith method from FAO (Equation (11)) was used since it has been approved by many researchers as a standard method for calculating the reference evapotranspiration [42]. This method was also used to measure reference plant evaporation in the study area and showed the lowest error when compared to other methods such as Hargreaves [43].

$$ET_o = \frac{0.408\Delta(R_n - G_o) + \gamma \frac{C_n}{T+273} U_2 (e_s - e_a)}{\Delta + \gamma(1 + C_d U_2)} \quad (11)$$

where ET_o is reference evapotranspiration (mm/day), R_n is the net radiation on the plant surface ($\text{MJ}/\text{m}^2 \cdot \text{day}$), G_o stands for soil heat flux ($\text{MJ}/\text{m}^2 \cdot \text{day}$), T is average air temperature at a height of 2 m ($^{\circ}\text{C}$), U_2 is wind speed at a height of two meters (m/s), e_s is saturated vapor pressure (kPa) and e_a is actual vapor pressure (kPa), Δ is slope of the vapor pressure curve ($\text{kPa}/^{\circ}\text{C}$), γ is psychrometric constant coefficient ($\text{kPa}/^{\circ}\text{C}$), C_n and C_d are constant coefficients determined according to the type of reference plant and the calculation period, respectively. In the present study, the parameters needed to calculate ET_{ins} are obtained from the meteorological station located in the field.

2.3.3. Estimation of Standard Evapotranspiration

According to the FAO 56 guidelines, evapotranspiration of plants can be measured under standard or non-standard conditions. In standard conditions, there is no limitation on plant growth or evapotranspiration under the influence of salinity and water stress, low crop density, pests and diseases, weeds or low soil fertility [42]. The standard plant evapotranspiration (ET_c) is calculated by multiplying the reference evapotranspiration (ET_o) by the plant coefficient (K_c) according to Equation (12) [42].

$$ET_c = K_c \times ET_o \quad (12)$$

Two methods for calculating crop standard ET are stated in the FAO 56 guidelines [41]: the one-component plant coefficient method (Equation (12)) and the two-component method. In the one-component method, ET of plants is obtained by multiplying reference evapotranspiration (ET_o) by the crop coefficient (K_c), whereas in the two-component method, two separate factors are presented to describe the difference between the evaporation from the soil surface (K_e) and transpiration from the plant surface (K_{cb}) [41]. Therefore, evaporation and transpiration are determined by the two-component method using Equation (13). Considering that irrigation in the farm is performed by the bubbler pressure irrigation system, the evaporation and transpiration from the soil surface or empty space between trees is close to zero. As a result, K_e is zero in the present study. So, using Equation (12) or (13) does not make a difference in the studied farm.

$$ET_c = (K_{cb} + K_e) \times ET_o \quad (13)$$

The two-component crop coefficient method has more calculation steps compared to the one-component method. Under non-standard conditions, with the reduction in ground water potential energy below the threshold value, the plant is subject to water stress. The effect of water stress on evaporation and transpiration is shown by multiplying the water stress coefficient (K_s) by the basic crop coefficient (K_{cb}) following Equation (14) [42].

$$ET_{c_adj} = (K_s \times K_{cb} + K_e) \times ET_o \quad (14)$$

Based on Equation (12), it is possible to obtain the real K_c value in the form of an image by dividing the actual instant evapotranspiration (ET_{ins}) obtained from the SEBAL algorithm on the day of the satellite passage by the ET_o on that day.

According to Equation (9), in the SEBAL algorithm the reference evaporation fraction (ETrF) can be defined as the instantaneous crop coefficient (K_{c-int}), because when ETrF is multiplied by the evapotranspiration of the reference plant (ET_o), the actual amount of evapotranspiration (ET_{ins} or ET_{a-ins}) will be obtained. When the actual evapotranspiration is calculated through the SEBAL algorithm (ET_a) and the standard evapotranspiration based on the FAO 56 guidelines (ET_c), the trees under drought stress can be identified by examining the difference between both values. As mentioned, the crop coefficient (K_c) is needed to calculate standard evaporation (ET_c). The crop coefficient varies according to plant type, climate and plant development stages [42].

Although the study farm is covered with pistachio plant species, due to the difference in canopy percentage, leaf area index, plan age and height, albedo, aerodynamic conditions, etc., it is not possible to consider the same crop coefficient for the entire farm. To solve this limitation, in the present study, the relationship between ETrF (K_{c-int}) and NDVI is used. Through this relationship, the optimum crop coefficient (K_c) and then standard evaporation were calculated. The optimum crop coefficient is actually the same linear regression relationship between NDVI and K_{c-int} , which shows how much K_c should be for each NDVI level. The minimum crop coefficient for each NDVI shows the basic crop coefficient (K_{cb}).

3. Results

3.1. Evapotranspiration in the Pistachio Farm

The actual ET map obtained through the SEBAL algorithm is shown in Figure 4. According to this map, in surfaces without pistachio trees, the actual ET is less than 2 mm/day. ET close to zero in the areas without trees is consistent with the bubbler pressure irrigation system in the farm. The maximum ET of 8 mm/day was obtained on 10 July 2022, in pistachio surface cover. The average daily ET from the pistachio trees was 4.3 mm/day, but the reference ET of this plant on this day was 6.7 mm/day. The different results are driven by the fact that the FAO 56 method multiplied the reference ET by the crop coefficient (Equation (12)).

Considering the phenology stage of pistachio trees (middle stage of growth), the weather and FAO 56 guidelines, the value of the crop coefficient (K_c) on the date of imaging was 1.17 for the whole farm. In general, according to the FAO 56 guidelines, the standard ET for this farm should be 7.8 mm/day. According to Figure 4, ET ranged between 7 and 8 mm/day in some pistachio rows, but it was less than 7 mm/day in some trees. Therefore, ET is different in each tree depending on, e.g., canopy cover and the leaf area index. As a result, it is necessary to first prepare a standard ET map and then compare the ET of each tree with the optimal ET value of the same tree.

3.2. The Crop Coefficient in the Pistachio Farm

The instantaneous crop coefficient map (ETrF in the SEBAL algorithm) is shown in Figure 5. According to this figure, the average crop coefficient in the entire farm with pistachio tree cover was 0.66, with a minimum of ~0.3 and a maximum of 1. According to Equation (12), based on the FAO 56 guidelines, the standard crop coefficient for the farm (1.17) and the average real crop coefficient of the farm (0.66), the stress factor (K_s) of the study area was 0.55. Hence, there exists water stress in the farm. However, to determine the areas with the highest stress, the relationship between NDVI and the crop coefficient was used.

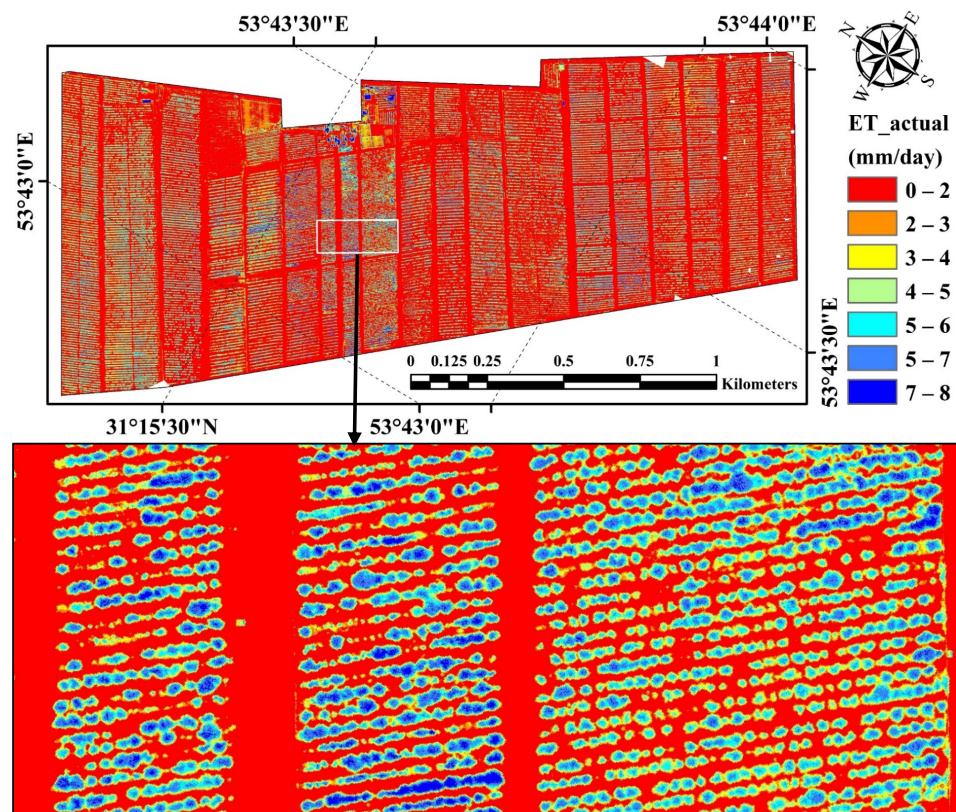


Figure 4. Actual evapotranspiration map obtained via the SEBAL algorithm on 10 July 2022, in the whole farm (top) and zooming in on the far plot (white box) (bottom).

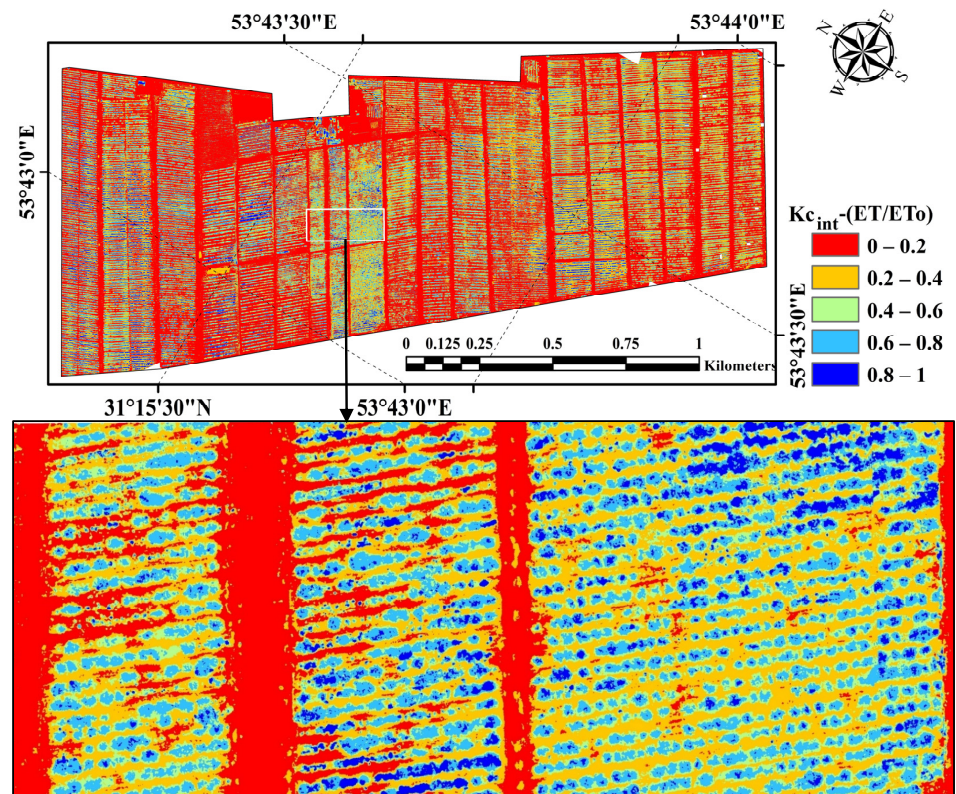


Figure 5. The instantaneous crop coefficient (K_{c-int}) of the studied farm on 10 July 2022 (top) and zooming in on the white box (bottom).

The relationship between the instantaneous crop coefficient (K_{c-int}) and the NDVI crop coefficient is shown in Figure 6. Considering that pixel size of the UAV images is 10 cm, the points in Figure 6 are very dense and scattered. However, it should be noted that there is a significant linear relationship between NDVI and K_{c-int} ($R^2 = 0.67, p < 0.01$). The relationship between K_{c-int} and NDVI helps to determine the minimum, average and maximum value of the crop coefficient for each NDVI value. In the present study, the average value or linear regression model was considered as the optimum crop coefficient (K_c).

By substituting the NDVI value in the relationship between the crop coefficient (K_{c-int}) and NDVI, the crop coefficient map was obtained in the optimal state for the farm, and by multiplying the crop coefficient map by the reference ET value of the pistachio (6.7 mm/day), the standard ET map was obtained (Figure 7). In Figure 7, in fact, the ET of each tree has been obtained according to the coverage level (i.e., NDVI). The minimum ET in areas without vegetation should be zero and the maximum in large trees, with high NDVI, should be 7 mm/day.

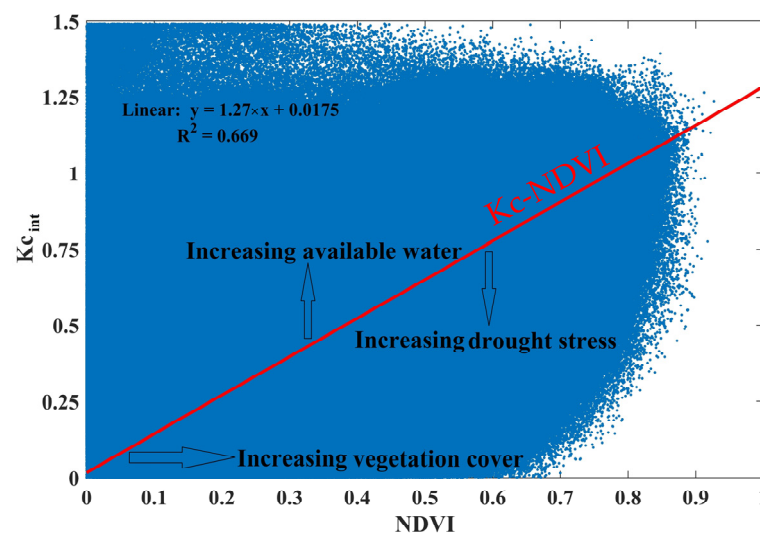


Figure 6. Relationship between the instantaneous crop coefficient (K_{c-int}) and NDVI.

3.3. Drought Stress in the Pistachio Farm

The drought stress map of the study area on 10 July 2022, is shown in Figure 8. This map is the difference between the actual evapotranspiration map (Figure 4) and the standard evapotranspiration (Figure 7). In Figures 4 and 7 the farm soil is placed in the class 0–2 mm of evaporation and transpiration (image background), and thus in Figure 8, the areas without pistachio trees or the field soil ($NDVI < 0.2$) are displayed as background to clearly show the trees and improve the accuracy of drought stress map. According to Figure 8, although in general the ET of the farm is close to normal conditions and the actual evapotranspiration (ET_a) is higher than the standard evapotranspiration (ET_{st}), drought stress conditions are observed in some rows and trees (negative values with yellow, orange and red colors). In the present study, some of the stress points in the map were further investigated through field visits. For example, in point 1, a row of trees with stress is shown (Figure 8). According to the field visits, signs of stress (e.g., small and sunburned leaves) were observed in this row, which was caused by the failure of the irrigation system and the high intensity of the pistachio psyllium pest (Figure 9A,D). At point 2, a semi-dried and stressed tree was observed, which according to the field visits was caused by the strain of the irrigation system (Figure 9B,C).

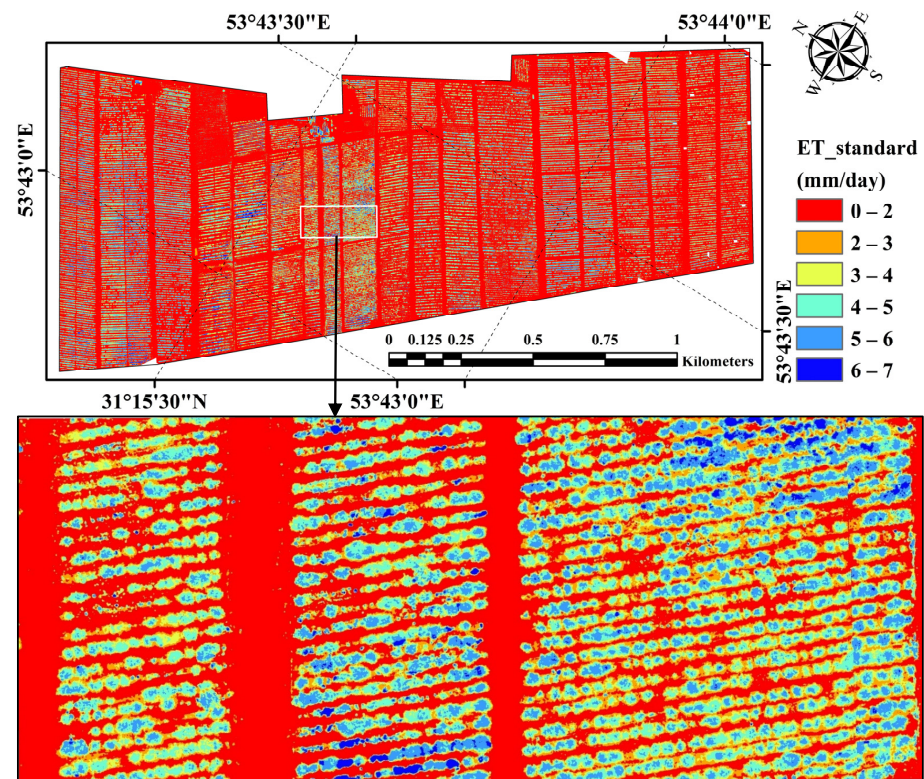


Figure 7. Standard evapotranspiration obtained through the relationship between K_c and NDVI on 10 July 2022, in the whole farm (top) and zooming in on the white box (bottom).

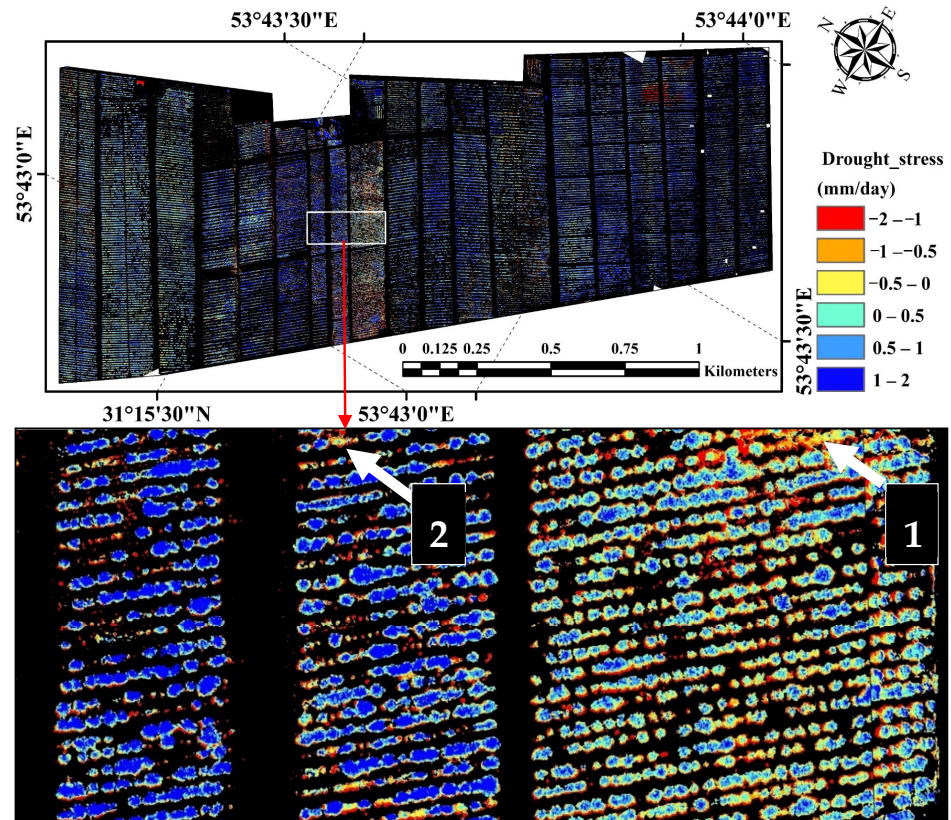


Figure 8. Farm drought stress map based on the difference between actual evapotranspiration and standard evapotranspiration, on 10 July 2022, in the whole farm (top) and zooming in on the white box (bottom).

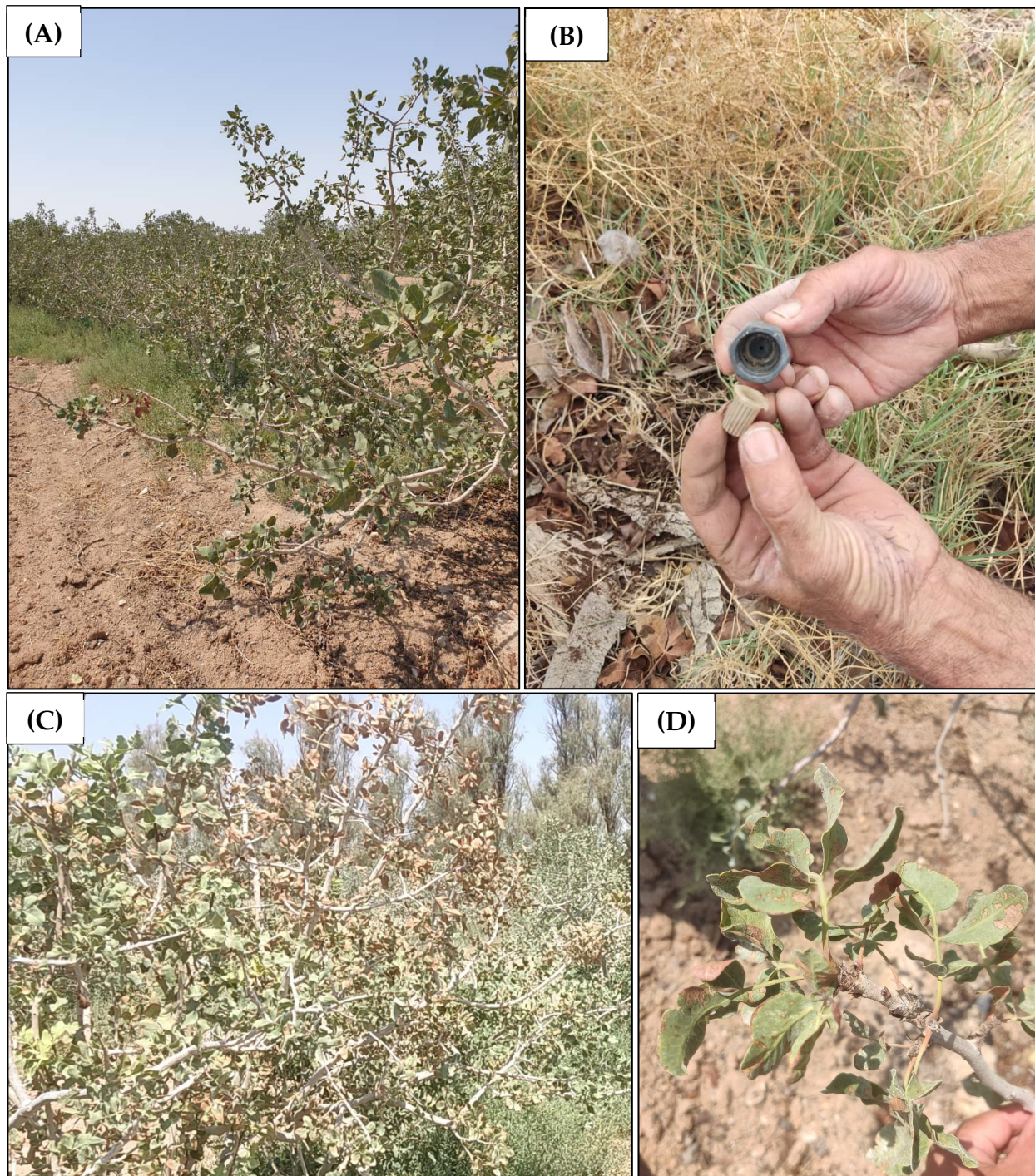


Figure 9. Observation of drought stress for validation of sites identified in Figure 8. (A) signs of small and sunburned leaves and no new annual growth; (B) straining of the pressurized irrigation system; (C) semi-drying of the pistachio tree; and (D) the effect of psyllid pest (*Agonoscena pistaci*) on pistachio leaves.

4. Discussion

UAVs have been widely and successfully used in precision agriculture research [44–46]. In the present study, actual evapotranspiration on 10 July 2022 was obtained using the SEBAL algorithm. In general, the average evapotranspiration in pistachio trees within the farm was 4.3 mm/day and the maximum was 8 mm/day. The reference ET of pistachio on the collected images was 6.7 mm/day, and considering the standard crop coefficient

according to the FAO 56 guidelines (1.17), the standard evapotranspiration for this farm was 7.8 mm/day. The standard evapotranspiration value according to the FAO 56 guidelines corresponds to the actual maximum evapotranspiration value on the farm. In other words, in areas and trees where the farm conditions are close to the standard ET conditions, the actual evapotranspiration of SEBAL is in full compliance with the FAO 56 guidelines. However, in the present study, measured evaporation data (e.g., through lysimeters) were not available to validate the results of the SEBAL algorithm. Numerous studies have been conducted in Iran to evaluate the accuracy of the SEBAL algorithm. In farms located at the edge of the Abarkoh desert, in Yazd province (the same study area; Figure 1), in an area extending over 3160 ha, the actual evapotranspiration of pistachio trees was 6 mm/day based on Landsat 8 satellite images taken from 1 to 15 July 2017 [43]. The difference between the values obtained in the present study (4.3 mm/day) and the study by Ghafarian et al. [43] is due to the modification in the spatial resolution of Landsat 8 images and the UAV image, and the difference in the irrigation system in the studied farm (flood irrigation vs. bubbler pressure irrigation systems). In Semnan province, Iran, evapotranspiration of pistachio trees estimated to be 5 and 6 mm/day when using the SEBAL algorithm and Landsat 8 images, respectively, in July 2013 and 2016 [47]. In Markazi province, Iran, evapotranspiration values of pistachio trees were 3.8 and 4.1 mm/day when using the SEBAL algorithm and Landsat 8 images, measured on 15 and 31 July 2018, respectively [48].

One of the simple and successful methods for determining the evaporation of plants and crops is the method mentioned in the FAO 56 guidelines [42]. However, it is difficult to estimate K_c , especially when the study area is heterogeneous in terms of variables such as coverage. In the present study, the relationship between the pistachio crop coefficient and NDVI was investigated. The results show a significant correlation between both ($p < 0.01$). Previous research has also shown significant correlation between the crop coefficient of different crops and crop coefficients in time (length of a growing season) and place (at the farm scale) [37,49–53]. In our study area, the crop coefficient of pistachio trees ranged between 0.3 and 1 according to the value of NDVI. The standard crop coefficient of pistachio in the middle period of growth, according to the FAO 56 guidelines, reaches 1.2 in the studied area [42]. However, the results of this study show that the average crop coefficient of pistachios in the investigated farm is 0.66. The difference between the standard crop coefficient and the actual crop coefficient in the farm can occur for two reasons. First, the pistachio crop coefficients based on the FAO 56 guidelines are not accurate for Iran's conditions, and secondly, the difference in the standard and actual crop coefficients is because of the stress coefficient (K_s) (Equation (13)). In previous studies, the accuracy of different evaporation algorithms was evaluated using the FAO 56 without considering the stress coefficient (i.e., drought or salinity stress). It should be noticed that the stress coefficients must be considered to estimate the real ET values [31], but they are not accounting for the standard ET calculation (Equation (11)) although in many farms the ET conditions are far from the standard conditions of FAO 56. The lack of field measurements to validate the measured ET using imaging from UAV is a limitation of this study, and also common in similar studies [48].

In the pistachio farms of Yazd province, Iran, the study in [43] showed that there is a significant correlation between the crop coefficient and NDVI in different stages of pistachio growth ($p < 0.01$), using Landsat 8 images. In this study, the pistachio crop coefficient ranged between 0.3 and 0.9. Also, the relationship between K_c and NDVI during the growth development stage (1 June to 15 July) was obtained as $K_c = 1.29 \times \text{NDVI} + 0.338$. Focusing on corn in Mongolia, the study in [32] showed a significant correlation between the vegetation factor and the crop coefficient when estimating the crop coefficient using UAV multispectral images. This study also demonstrated that the crop coefficient obtained from the regression models with the vegetation factors compared to the crop coefficient calculated from in situ measurements has a greater ability to evaluate irrigation management in terms of field and crop diversity. As mentioned, there is a correlation between the changes in the crop coefficient in time and place with most of the vegetation factors. However, the degree

of correlation and regression model will be different for different crop coefficients, crops and regions. For example, the relationship between K_c and NDVI was $K_c = 1.62 \times \text{NDVI} - 0.14$ and $K_c = 2.11 \times \text{NDVI} - 0.49$ on corn and alfalfa crops, respectively [51]. In another study, the relationship between K_c and NDVI for different agricultural crops was obtained as $K_c = 1.457 \times \text{NDVI} - 0.17$ [54].

Many studies have focused on measuring evaporation and transpiration from farming fields. However, improving water management is still a challenge, especially due to the need to identify the specific areas with drought stress at fine scale. By determining the relationship between vegetation indices and evaporation and transpiration, the minimum evaporation and transpiration or vegetation coefficient can be determined on the field at the plant scale, and by comparing the actual evaporation and transpiration values with the required minimum evaporation and transpiration we can assess drought stress of each tree. Since water evaporation is an energy-consuming process, increasing the rate of evaporation and transpiration causes a decrease in the surface temperature of leaves and plants. Based on this principle, the existence of thermal images is one of the most important requirements for estimating evaporation and transpiration and drought stress using the surface energy balance equation.

Generally, the use of correlation models between remotely sensed vegetation factors and the crop coefficient allows considerations about the heterogeneity and temporal and spatial changes in vegetation cover across relatively large scales (e.g., different farms and agricultural crops). It also provides crop coefficient maps of the study area, which are relevant to improve irrigation management and prevent plant stress effectively. The methodology developed can be used for different types of orchard farms in arid and semi-arid regions. This could provide a relevant contribution to improve water use efficiency, particularly relevant in water-scarce regions, and support crop yield and production quality under climate change conditions.

5. Conclusions

This study uses high-resolution UAV multispectral and thermal images of a pistachio farm in Yazd province, Iran, to calculate evapotranspiration and assess drought stress of individual trees, and map the spatial heterogeneity at the farm scale. The use of remote sensing techniques (multispectral drone images) to calculate actual evapotranspiration through the SEBAL algorithm, in combination with reference evapotranspiration of the plant following the FAO 56 guidelines, is a suitable method to estimate evaporation and drought stress of pistachio at the level of a single tree, as confirmed by field observations.

This study showed that the minimum, maximum and average evaporation and transpiration of pistachio trees in the study farm were 3, 8 and 4.3 mm/day on 10 July 2022. In general, the amount of evaporation and transpiration in the field was lower than the recommended amount based on the FAO 56 guidelines (7.8 mm per day) in some trees, which indicates the existence of drought stress conditions in specific areas. Environmental heterogeneities of the field (such as soil texture), age and size of trees cause part of the difference in evaporation and transpiration values (from 3 to 8 mm/day). Therefore, field heterogeneity should be considered to identify trees under drought stress. The findings showed that it is possible to obtain the optimal or standard crop coefficient and evapotranspiration for each level of NDVI by using the regression model between NDVI and the crop coefficient.

Consequently, it is possible to prepare crop coefficient maps for heterogeneous surfaces using NDVI in different crop growth stages. Additionally, the standard evapotranspiration value of the crop can be obtained by multiplying the evapotranspiration value of the reference plant in the desired interval. However, it should be noted that these relationships are different for each crop and region. Evapotranspiration maps can be obtained with high resolution, and thus be used for precision agriculture. Providing real-time and high-resolution data on drought stress in farming systems is extremely relevant to improve irrigation management in water-scarce regions, such as arid and semi-arid areas.

Author Contributions: Conceptualization, H.Z.K. and H.R.G.M.; methodology, H.Z.K. and H.R.G.M.; validation, H.Z.K., H.R.G.M. and C.S.S.F.; formal analysis, H.Z.K., H.R.G.M. and C.S.S.F.; investigation, H.Z.K. and H.R.G.M.; data curation, H.R.G.M.; writing—original draft preparation, H.Z.K.; writing—review and editing, H.Z.K., H.R.G.M. and C.S.S.F.; supervision, H.R.G.M. All authors have read and agreed to the published version of the manuscript.

Funding: C. Ferreira acknowledges the financial support provided by the Portuguese Foundation for Science and Technology, P.I., through the institutional scientific employment program-contract (CEEC-INST/00077/2021) and the project PTDC/EEI-ROB/2459/2021.

Data Availability Statement: The data presented in this study are available on request from the corresponding author because it contains information that could compromise the privacy of research participants.

Conflicts of Interest: The authors declare no conflicts of interest.

References

1. Yang, Y.; Qiu, J.; Zhang, R.; Huang, S.; Chen, S.; Wang, H.; Luo, J.; Fan, Y. Intercomparison of three two-source energy balance models for partitioning evaporation and transpiration in semiarid climates. *Remote Sens.* **2018**, *10*, 1149. [\[CrossRef\]](#)
2. Bezerra, B.G.; Santos, C.A.C.; Silva, B.B.; Perez-Marin, A.M.; Bezerra, M.V.C.; Bezerra, J.R.C.; Ramana Rao, T.V. Estimation of Soil Moisture in the Root-Zone from Remote Sensing Data. *Rev. Bras. Ciênc. Solo* **2013**, *37*, 595–603. [\[CrossRef\]](#)
3. Wang, K.; Dickinson, R.E. A review of global terrestrial evapotranspiration: Observation, modeling, climatology, and climatic variability. *Rev. Geophys.* **2012**, *50*, 1–54. [\[CrossRef\]](#)
4. Niu, H.; Zhao, T.; Wang, D.; Chen, Y. Estimating evapotranspiration with UAVs in agriculture: A review. In Proceedings of the 2019 ASABE Annual International Meeting, Boston, MA, USA, 7–10 July 2019; American Society of Agricultural and Biological Engineers: St. Joseph, MI, USA, 2019; p. 1.
5. Allen, R.; Irmak, A.; Trezza, R.; Hendrickx, J.M.; Bastiaanssen, W.; Kjaersgaard, J. Satellite-based ET estimation in agriculture using SEBAL and METRIC. *Hydrol. Proc.* **2011**, *25*, 4011–4027. [\[CrossRef\]](#)
6. Liou, Y.A.; Kar, S.K. Evapotranspiration estimation with remote sensing and various surface energy balance algorithms—A review. *Energies* **2014**, *7*, 2821–2849. [\[CrossRef\]](#)
7. Zare khormizi, H.; Tavili, A.; Ghafarian Malamiri, H.R. Estimation of Actual Evapotranspiration Using SEBAL Algorithm and Comparison with Improved FAO 56 Standard Evapotranspiration with KC-NDVI Relationship. *Iran. J. Remote Sens. GIS* **2021**, *13*, 73–92. [\[CrossRef\]](#)
8. French, A.N.; Sanchez, C.A.; Wirth, T.; Scott, A.; Shields, J.W.; Bautista, E.; Saber, M.N.; Wisniewski, E.; Gohardoust, M.R. Remote sensing of evapotranspiration for irrigated crops at Yuma, Arizona, USA. *Agric. Water Manag.* **2023**, *290*, 108582. [\[CrossRef\]](#)
9. Liu, Y.; Zhao, Y.; Zhai, J.; Liang, H.; Zhu, Y.; Wang, Y.; Wang, Q.; Li, X.; Yu, J. Exploring evapotranspiration stress in China: A blending approach employing multi-source remote sensing proxies. *J. Hydrol. Reg. Studies* **2024**, *51*, 101653. [\[CrossRef\]](#)
10. Soni, A.K.; Tripathi, J.N.; Ghosh, K.; Singh, P.; Sateesh, M.; Singh, K.K. Estimation of regional-scale near real time reference evapotranspiration using remote sensing and weather data to improve agriculture advisory. *Earth Sci. Inf.* **2024**, *17*, 679–697. [\[CrossRef\]](#)
11. Zare khormizi, H.; Hosseini, S.Z.; Mokhtari, M.H.; Ghafarian Malamiri, H.R. Reconstruction of MODIS NDVI Time Series using Harmonic AN alysis of Time Series algorithm (HANTS). *MJSP* **2017**, *21*, 221–255.
12. Su, Z. The Surface Energy Balance System (SEBS) for estimation of turbulent heat fluxes. *Hydrol. Earth Syst. Sc. Disc.* **2002**, *6*, 85–100. [\[CrossRef\]](#)
13. Bastiaanssen, W.G.; Menenti, M.; Feddes, R.A.; Holtslag, A.A.M. A remote sensing surface energy balance algorithm for land (SEBAL). 1. Formulation. *J. Hydrol.* **1998**, *212*, 198–212. [\[CrossRef\]](#)
14. Menenti, M.; Choudhury, B.J. Parameterization of land surface evapotranspiration using a location dependent potential evapotranspiration and surface temperature range. Exchange processes at the land surface for a range of space and time scales. *J. Glob.* **1993**, *212*, 561–568.
15. Allen, R.G.; Tasumi, M.; Trezza, R. Satellite-based energy balance for mapping evapotranspiration with internalized calibration (METRIC)-Model. *J. Irrig. Drain.* **2007**, *133*, 380–394. [\[CrossRef\]](#)
16. Kustas, W.P.; Norman, J.M. Evaluation of soil and vegetation heat flux predictions using a simple two-source model with radiometric temperatures for partial canopy cover. *Agric. For. Meteorol.* **1999**, *94*, 13–29. [\[CrossRef\]](#)
17. Bastiaanssen, W.G.M. SEBALbased sensible and latent heat fluxes in the irrigated Gediz Basin, Turkey. *J. Hydrol.* **2000**, *229*, 87–100. [\[CrossRef\]](#)
18. Ghafarian Malamiri, H.R.; Zare Khormizi, H.; Mortaz, M. Estimation of actual evapotranspiration of pistachio plants using the SEBAL algorithm and Landsat 8 images: A case study of Abarkooh desert margin in Yazd Province. *J. Geog. Res. Desert Areas* **2021**, *8*, 51–82.
19. Sane, M.; Kouchakzadeh, M.; Sharifi, F. Evaluation of SEBAL Algorithm for Estimation of Real Evapotranspiration in Vardij area. *Iran. J. Irrig. Drain.* **2020**, *14*, 125–135.

20. Moqbeli damane, M.; Sanaei nejad, H.; Kafash, M. Evaluation of SEBAL algorithm for actual evapotranspiration estimating by using Landsat 8 images in multiple land use landscape (Case study: Freeman area). *J. Clim. Res.* **2022**, *1401*, 165–182.
21. Bala, A.; Rawat, K.S.; Misra, A.K.; Srivastava, A. Assessment and validation of evapotranspiration using SEBAL algorithm and Lysimeter data of IARI agricultural farm, India. *Geocarto Int.* **2016**, *31*, 739–764. [[CrossRef](#)]
22. Rawat, K.S.; Bala, A.; Singh, S.K.; Pal, R.K. Quantification of wheat crop evapotranspiration and mapping: A case study from Bhiwani District of Haryana, India. *Agric. Water Manag.* **2017**, *187*, 200–209. [[CrossRef](#)]
23. Elnmer, A.; Khadr, M.; Kanae, S.; Tawfik, A. Mapping daily and seasonally evapotranspiration using remote sensing techniques over the Nile delta. *Agric. Water Manag.* **2019**, *213*, 682–692. [[CrossRef](#)]
24. Laipelt, L.; Kayser, R.H.B.; Fleischmann, A.S.; Ruhoff, A.; Bastiaanssen, W.; Erickson, T.A.; Melton, F. Long-term monitoring of evapotranspiration using the SEBAL algorithm and Google Earth Engine cloud computing. *ISPRS J. Photogramm. Remote Sens.* **2021**, *178*, 81–96. [[CrossRef](#)]
25. Fawzy, H.E.D.; Sakr, A.; El-Enany, M.; Moghazy, H.M. Spatiotemporal assessment of actual evapotranspiration using satellite remote sensing technique in the Nile Delta, Egypt. *Alex. Eng. J.* **2021**, *60*, 1421–1432. [[CrossRef](#)]
26. Park, S.; Ryu, D.; Fuentes, S.; Chung, H.; O’Connell, M.; Kim, J. Mapping Very-High-Resolution Evapotranspiration from Unmanned Aerial Vehicle (UAV) Imagery. *ISPRS Int. J. Geo-Inf.* **2021**, *10*, 211. [[CrossRef](#)]
27. Xia, T.; Kustas, W.P.; Anderson, M.C.; Alfieri, J.G.; Gao, F.; McKee, L.; Prueger, J.H.; Geli, H.M.E.; Neale, C.M.U.; Sanchez, L.; et al. Mapping evapotranspiration with high-resolution aircraft imagery over vineyards using one-and two-source modeling schemes. *Hydrol. Earth Syst. Sc.* **2016**, *20*, 1523–1545. [[CrossRef](#)]
28. Ghafarian Malamiri, H.R.; Zare Khormizie, H. Reconstruction of cloud-free time series satellite observations of land surface temperature (LST) using harmonic analysis of time series algorithm (HANTS). *J. GIS RS Nat. Res.* **2017**, *8*, 37–55.
29. Ghafarian Malamiri, H.R.; Zare, H.; Rousta, I.; Olafsson, H.; Izquierdo Verdiguier, E.; Zhang, H.; Mushore, T.D. Comparison of harmonic analysis of time series (HANTS) and multi-singular spectrum analysis (M-SSA) in reconstruction of long-gap missing data in NDVI time series. *Remote Sens.* **2020**, *12*, 2747. [[CrossRef](#)]
30. Dong, X.; Zhang, Z.; Yu, R.; Tian, Q.; Zhu, X. Extraction of information about individual trees from high-spatial-resolution UAV-acquired images of an orchard. *Remote Sens.* **2020**, *12*, 133. [[CrossRef](#)]
31. Bellvert, J.; Zarco-Tejada, P.J.; Girona, J.; Fereres, E.J.P.A. Mapping crop water stress index in a ‘Pinot-noir’ vineyard: Comparing ground measurements with thermal remote sensing imagery from an unmanned aerial vehicle. *Precis. Agric.* **2014**, *15*, 361–376. [[CrossRef](#)]
32. Zhang, Y.; Han, W.; Niu, X.; Li, G. Maize crop coefficient estimated from UAV-measured multispectral vegetation indices. *Sensors* **2019**, *19*, 5250. [[CrossRef](#)] [[PubMed](#)]
33. Mateen, A.; Zhu, Q. Weed detection in wheat crop using UAV for precision agriculture. *Pak. J. Agric. Sci.* **2019**, *56*, 809–817.
34. Barros, T.; Conde, C.; Gonçalves, G.; Premebida, C.; Monteiro, M.; Ferreira, C.S.S.; Nunes, U. Multispectral vineyard segmentation: A deep learning comparison study. *Comput. Electron. Agric.* **2022**, *195*, 106782. [[CrossRef](#)]
35. Vanegas, F.; Bratanov, D.; Powell, K.; Weiss, J.; Gonzalez, F. A novel methodology for improving plant pest surveillance in vineyards and crops using UAV-based hyperspectral and spatial data. *Sensors* **2018**, *18*, 260. [[CrossRef](#)] [[PubMed](#)]
36. Mokhtari, A.; Ahmadi, A.; Daccache, A.; Drechsler, K. Actual evapotranspiration from UAV images: A multi-sensor data fusion approach. *Remote Sens.* **2021**, *13*, 2315. [[CrossRef](#)]
37. Niu, H.; Zhao, T.; Wei, J.; Wang, D.; Chen, Y. Reliable Tree-level Evapotranspiration Estimation of Pomegranate Trees Using Lysimeter and UAV Multispectral Imagery. In Proceedings of the 2021 IEEE Conference on Technologies for Sustainability (SusTech), Irvine, CA, USA, 22–24 April 2021; pp. 1–6.
38. Ortega-Farías, S.; Ortega-Salazar, S.; Poblete, T.; Poblete-Echeverría, C.; Zúñiga, M.; Sepúlveda-Reyes, D.; Kilic, A.; Allen, R. Estimation of olive evapotranspiration using multispectral and thermal sensors placed aboard an unmanned aerial vehicle. In Proceedings of the VIII International Symposium on Irrigation of Horticultural Crops, Lleida, Spain, 8–11 June 2015; pp. 1–8.
39. Tang, J.; Han, W.; Zhang, L. UAV multispectral imagery combined with the FAO-56 dual approach for maize evapotranspiration mapping in the north China Plain. *Remote Sens.* **2019**, *11*, 2519. [[CrossRef](#)]
40. Allen, R.G.; Waters, R.; Tasumi, M.; Trezza, R.; Bastiaanssen, W. SEBAL, Surface Energy Balance Algorithms for Land, Idaho Implementation, Version 1.0. *Advanced Training and User’s Manual*. 2002. Available online: <https://posmet.ufv.br/wp-content/uploads/2017/04/MET-479-Waters-et-al-SEBAL.pdf> (accessed on 14 May 2024).
41. Rouse, J.W.; Haas, R.H.; Schell, J.A.; Deering, D.W. Monitoring vegetation systems in the Great Plains with ERTS. In Proceedings of the 3rd ERTS Symposium, NASA SP-351 I, Washington, DC, USA, 10–14 December 1973; pp. 309–317.
42. Allen, R.G.; Pereira, L.S.; Raes, D.; Smith, M. Crop evapotranspiration—Guidelines for computing crop water requirements—FAO Irrigation and drainage paper 56. *Fao Rome* **1998**, *300*, D05109.
43. Zare khormizi, H.; Ghafarian Malamiri, H.R. Estimation of Crop Coefficient and Pistachio Plant’s (*Pistacia vera* L.) KC-NDVI Relationship Using Remote Sensing (Case study: Pistachio orchards of Abarkuh desert margin, Yazd province). *Desert Manag.* **2020**, *8*, 101–120.
44. Radoglou-Grammatikis, P.; Sarigiannidis, P.; Lagkas, T.; Moscholios, I. A compilation of UAV applications for precision agriculture. *Comp. Net.* **2020**, *172*, 107148. [[CrossRef](#)]
45. Singh, P.K.; Sharma, A. An intelligent WSN-UAV-based IoT framework for precision agriculture application. *Comp. Electr. Eng.* **2022**, *100*, 107912. [[CrossRef](#)]

46. Raptis, E.K.; Englezos, K.; Kypris, O.; Krestenitis, M.; Kapoutsis, A.C.; Ioannidis, K.; Vrochidis, S.; Kosmatopoulos, E.B. CoFly: An automated, AI-based open-source platform for UAV precision agriculture applications. *SoftwareX* **2023**, *23*, 101414. [[CrossRef](#)]
47. Rahimzadegan, M.; Janani, A. Estimating evapotranspiration of pistachio crop based on SEBAL algorithm using Landsat 8 satellite imagery. *Agric. Water Manag.* **2019**, *217*, 383–390. [[CrossRef](#)]
48. Radiom, S. Estimation of actual evapotranspiration in pistachio orchards using SEBAL algorithm in three irrigation system. *J. RS GIS Nat. Res.* **2021**, *12*, 72–90.
49. Oliveira, T.C.D.; Ferreira, E.; Dantas, A.A.A. Temporal variation of normalized difference vegetation index (NDVI) and calculation of the crop coefficient (KC) from NDVI in areas cultivated with irrigated soybean. *Ciência Rural* **2016**, *46*, 1683–1688. [[CrossRef](#)]
50. El-Shirbeny, M.A.; Ali, A.M.; Badr, M.A.; Bauomy, E.M. Assessment of wheat crop coefficient using remote sensing techniques. *World J. Agric. Res.* **2014**, *1*, 12–17.
51. Reyes-Gonzalez, A.; Hay, C.; Kjaersgaard, J.; Neale, C. Use of remote sensing to generate crop coefficient and estimate actual crop evapotranspiration. In Proceedings of the 2015 ASABE Annual International Meeting, New Orleans, LA, USA, 26–29 July 2015; American Society of Agricultural and Biological Engineers: St. Joseph, Michigan, USA, 2015; p. 1.
52. Dingre, S.K.; Gorantiwar, S.D.; Kadam, S.A. Correlating the field water balance derived crop coefficient (Kc) and canopy reflectance-based NDVI for irrigated sugarcane. *Precis. Agric.* **2021**, *22*, 1134–1153. [[CrossRef](#)]
53. Elshikha, D.E.M.; Hunsaker, D.J.; Waller, P.M.; Thorp, K.R.; Dierig, D.; Wang, G.; Cruz, V.M.V.; Katterman, M.E.; Bronson, K.F.; Wall, G.W.; et al. Estimation of direct-seeded guayule cover, crop coefficient, and yield using UAS-based multispectral and RGB data. *Agric. Water Manag.* **2022**, *265*, 107540. [[CrossRef](#)]
54. Kamble, B.; Kilic, A.; Hubbard, K. Estimating crop coefficients using remote sensing-based vegetation index. *Remote Sens.* **2013**, *5*, 1588–1602. [[CrossRef](#)]

Disclaimer/Publisher’s Note: The statements, opinions and data contained in all publications are solely those of the individual author(s) and contributor(s) and not of MDPI and/or the editor(s). MDPI and/or the editor(s) disclaim responsibility for any injury to people or property resulting from any ideas, methods, instructions or products referred to in the content.